Plasma waveguides efficiently generated by Bessel beams in elongated cluster gas jets

H. Sheng, K. Y. Kim, V. Kumarappan, B. D. Layer, and H. M. Milchberg
Institute for Physical Science and Technology, University of Maryland, College Park, Maryland 20742, USA
(Received 27 May 2005; published 21 September 2005)

We demonstrate the efficient generation of plasma waveguides in elongated cluster gas jets using 100 ps axicon-generated Bessel beam pump pulses. The plasma waveguide space and time evolution is measured using picosecond interferometry. Small radius waveguides with central densities as low as $\sim 10^{18}$ cm^{-3} can be generated with this technique. Despite the expected subpicosecond cluster disassembly time, we observe long pulse absorption efficiencies that can be more than a factor of 10 greater than in unclustered gas targets of the same volume average atomic density. The maximum long pulse absorption observed in cluster jets under our range of conditions was 35%. The explanation for the enhanced absorption is that in the far-leading edge of the laser pulse, the volume of heated clusters evolves to a locally uniform and cool plasma already near ionization saturation, which is then heated by the remainder of the pulse. From this perspective, the use of clustered gases is equivalent to a supercharged preionization scheme for long duration laser pulses.

DOI: 10.1103/PhysRevE.72.036411 PACS number(s): 52.38.Hb, 36.40.Gk, 36.40.Vz, 52.50.Jm

I. INTRODUCTION

Optical guiding in plasmas is increasingly a component of many experiments and applications involving ultraintense laser pulses. The increased interaction length at high intensity of an optically guided pulse is essential to applications, including laser-driven electron accelerators [1,2], nonlinear short wavelength generation [3], and soft x-ray amplification [4]. Guiding has been demonstrated in plasmas produced by electrical discharge in capillaries, both prefilled with gas [5] and not [6], in imploding Z pinches [7], and by plasma structures generated through laser-driven nonequilibrium radial shock waves in gas targets [8] and in variations of this technique [9,10]. In addition, short waveguides have been generated by ponderomotive force expulsion of electrons by relativistically self-guided pulses [11]. Most recently, highly ionized waveguides have been generated in clustered gases, with long waveguide plasmas generated through the plasma evolution following the self-guiding and strong coupling [12] of a pulse injected into the end of a long cluster gas jet [13]. In that experiment, plasma waveguides were efficiently generated with millijoule level femtosecond pulses, which experienced absorptions up to 85%.

In this paper, we show that plasma waveguides can be also generated in clustered gases by line focusing a much longer duration laser pulse into an extended clustered gas jet. Previously, the line-focus technique has been limited to heating unclustered backfill or gas jet targets with line-focused pulses produced by axicons (Bessel beam heating) [8,10,14] or by cylindrical lenses [9], but pump absorption efficiency in these targets is typically less than a few percent. For very high backfill gas densities at atmospheric pressure and beyond ($>3\times 10^{19}$ atoms/cm^{-3}) absorption can be $\sim$10%, but the resulting electron densities can be much too high for some applications such as laser-driven resonant wakefield acceleration [1]. As a special case for Bessel beams, there are some pressure ranges in nonclustered gases where absorption can be resonantly increased depending on axicon geometry, pump laser intensity, pulsewidth, and wavelength [14], but absorption still remains below $\sim$15%, and the choice of target gas density is limited by the resonance condition.

In this paper we show that using clustered gas targets and long 100 ps heating pulses, absorption can be nonresonantly increased by as much as a factor of $\sim$10 compared to unclustered gases of the same volume average atomic density. We measure maximum long pulse absorption of 35%, which is only 2 to 3 times less than the absorption levels of femtosecond pulses. Using clustered gas targets and long pulse irradiation, we can make small diameter plasma waveguides with on-axis electron densities near 10^{18} cm^{-3}, significantly lower than with nonclustered targets. A 100 ps pulse appears to be a surprisingly efficient heater of the cluster plasma, despite the fact that individual clusters disassemble to below critical density on a time scale of only a few hundred femtoseconds, and thus are expected to be strongly absorbing only during that period [15].

In unclustered gas, efficient collisional breakdown for plasma waveguide generation requires high gas density N_0 due to the early time exponential growth of electron density $N_e(t)\sim N_{e0}\exp(SN_0t)$ where N_{e0} is the initial electron density and S is the collisional ionization rate. N_{e0} can be generated by optical field ionization (OFI) [16] in the main heating pulse, or through the use of a separate prepulse [9]. Alternatively, it can be provided by an auxiliary electrical discharge [10] in advance of a laser heater pulse.

In most practical cases, N_{e0} constitutes only a very small prefactor such that $Z_{init}=N_{e0}/N_0\ll 1$, where Z_{init} is the initial effective degree of ionization. Under these conditions, after enough e-folding times of N_e growth, saturation begins and the memory of N_{e0} is lost, with N_0 as the dominant factor in determining the end condition [17,18]. The requirement for large N_0 results in typical minimum electron densities in plasma waveguides, after radial hydrodynamic expansion, higher than $\sim 5\times 10^{18}$ cm^{-3}, which is not optimum for some applications, most notably resonant laser wakefield acceleration. For resonant excitation of wakefields, the goal is to match the laser pulse width to the plasma period. For 50–100 fs pulses, typical of today's high-power Ti:Sapphire

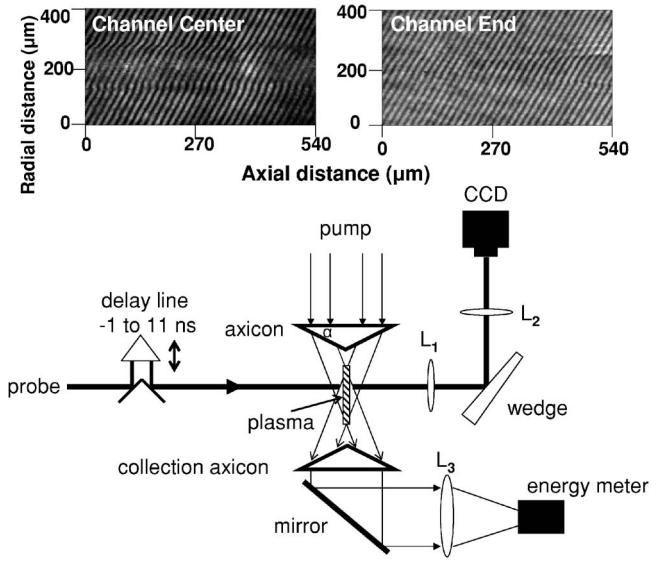

FIG. 1. Experimental setup, showing waveguide generating axicon with base angle $\alpha=25$ deg and folded wave front interferometer with variably delayed 1064 nm, 100 ps, ~1 mJ probe pulse, imaging optics and reflection wedge. The collection axicon is used for pump absorption measurements. The insets show typical interferograms of the central region of the waveguide and the end.

laser systems, the desirable electron density is $\sim 10^{18}$ cm^{-3} or less [19]. Using clustered gas jet targets and 100 ps axicon-focused Bessel beam pulses, we can achieve long, efficiently generated plasma waveguides at such low densities. The use of clusters strongly increases the effective level of preionization so that $Z_{\text{init}} \gg 1$. Since further growth in ionization over most of the laser envelope starts near saturation, sensitivity to N_{e0} is no longer lost. This is discussed in more detail in Sec. IV.

The clusters in our experiment are assemblies of $\sim 10^3$ to 10^7 atoms held together by mutually induced polarization forces, or van der Waals bonding [20]. Such inter-atom forces become significant under sufficient gas cooling. In our experiment, the cooling and collision processes leading to cluster formation occur when high-pressure gas adiabatically expands into vacuum through a supersonic nozzle. Typical cluster radii a are in the range $\sim 10-100$ Å such that $ka \ll 1$, where k is the laser vacuum wave number. For greater numbers of atoms and larger values of a such that the assembly size approaches the laser wavelength, the convention has been to use the term *droplet* rather than *cluster*.

II. EXPERIMENTAL SETUP

Figure 1 shows the experimental setup. Cluster jets were produced using a pulsed valve and a slot nozzle with an exit orifice of dimension 0.5 mm by 1.2 cm. High valve backing pressures and low temperatures favor the formation of larger clusters. The pulsed valve body is encased in a liquid nitrogen-cooled copper jacket so that the pre-expansion gas can be cooled as low as −120 °C. Valve backing pressure and temperature ranged from 150 to 1200 psi and 150 K to room temperature. The valve temperature was finely controlled to within ±0.2 K of any set point in this temperature range by two solid-state cartridge heaters encased in the copper jacket, which operate in tandem with the liquid nitrogen cooling [21]. The density of the clusters in our jet occupies a wide range $\sim 10^{12}-10^{17}$ clusters/cm^3, and the volume-average electron density after heating by a laser pulse and subsequent cluster plasma expansion can be in the range $10^{16}-10^{20}$ cm^{-3}. This density control is achieved by controlling the cluster size and density through the valve backing pressure and temperature.

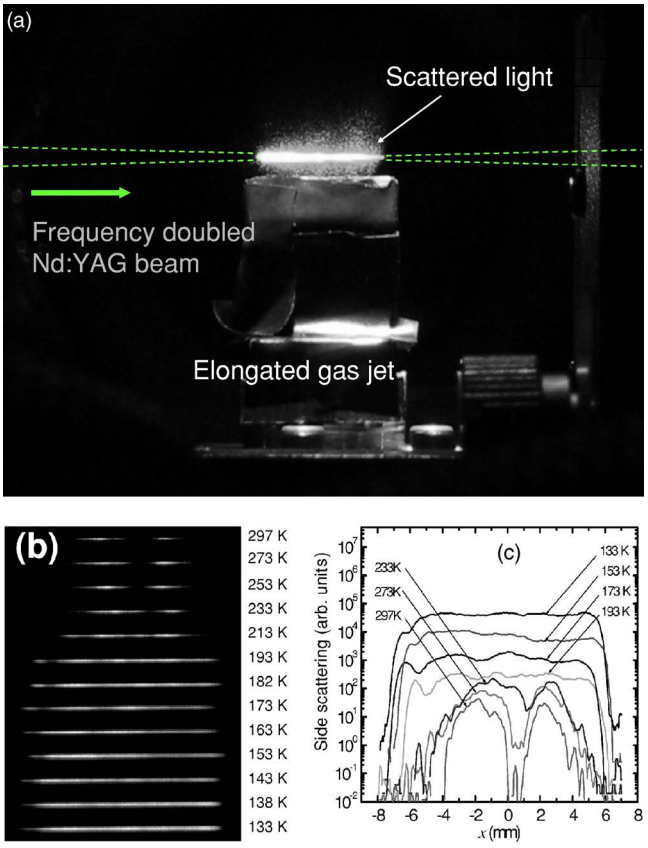

FIG. 2. (Color online) (a) Image of weak 532 nm beam scattered by elongated cluster jet. (b) Image of scattering zone of cluster jet versus valve temperature, for valve backing pressure of 400 psi. (c) Central lineout of the scattering images of (b). It is seen that the uniformity of the cluster flow improves with valve cooling.

An all-optical method to measure cluster size and density was developed to characterize cluster jets [22]. The method uses measurements of Rayleigh scattering and interferometry in combination. Figure 2(a) shows an image of a weak 10 ns duration 532 nm probe beam propagating along the long axis of the jet and scattering from clusters. A sequence of Rayleigh scattering images are shown in Fig. 2(b) for fixed backing pressure of 400 psi and variable valve temperature, with lineouts of these images seen in Fig. 2(c). It is seen that the cluster flow becomes quite uniform as the valve is cooled to 200 K and lower, and a very sharp ~0.5 mm falloff in scattering yield occurs at the ends of the jet. Figures 3(a) and 3(b) show a sequence of plots, obtained using the method of Ref. [22], of average cluster size and cluster number density as a function of valve backing pressure for four different

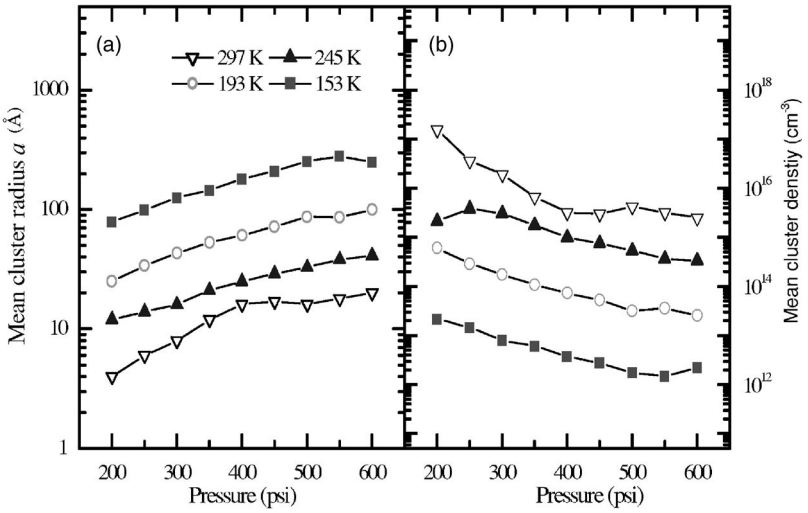

FIG. 3. Argon cluster (a) size and (b) density versus valve backing pressure for several valve temperatures. The measurement is made using the technique of Ref. [22].

valve temperatures. The wide control provided for cluster size and cluster density is evident.

The laser used in this experiment is a mode-locked Nd:YAG system with a wavelength of 1064 nm, pulse width of 100 ps, and energy up to 800 mJ. The pump beam was focused by an axicon with a base angle $\alpha=25$ deg, generating a ~ 1.3 cm long plasma column 2 mm above and along the axis of the cluster nozzle orifice. The beam resulting from focusing by the axicon, also called a Bessel beam [14], has a transverse profile invariant along the optical axis, while the length L along the optical axis of the high-intensity central maximum is determined by the beam radius a and the axicon base angle α according to $L=a(1/\tan\gamma-\tan\alpha)$, where $\gamma=\sin^{-1}(n\sin\alpha)$—$\alpha$ is the angle of approach of the axicon rays to the beam axis [18]. In our case $L=1.6$ cm for $\alpha=25$ deg, axicon BK-7 glass refractive index $n=1.507$ at $\lambda=1064$ nm, and $2a=1$ cm. The longitudinal intensity distribution along the axicon line focus has a peak located near the axial midrange and decreases toward the two ends. This occurs because the input beam profile is mapped onto the focal line with a radial weighting factor: the weighting factor is zero for the input beam center, which maps to a point closest to the axicon vertex, and the input beam periphery (where intensity decreases to zero) is mapped farthest from the axicon vertex [18]. In the experiment, the ends of the 1.6 cm long line focus overlap the ends of the cluster jet (as defined in the Rayleigh scattering images of Fig. 2(b)) so that there is no section of the jet left unionized. The peak vacuum intensity in the central maximum of the Bessel beam is $\sim 6\times 10^{13}$ W/cm^2 corresponding to the maximum laser energy used of 415 mJ, although in practice the breakdowns were more uniform with less energy. The range of intensities used is sufficient for the optical field ionization (OFI) of neutral argon. The OFI electrons act as a seed for the subsequent cascade avalanche ionization of the cluster. An image of the line breakdown in an elongated argon cluster jet is shown in Fig. 4. The ring on the screen at the left is nonlinear fluorescence of the locus of rays from the axicon that heat the plasma and are transmitted through it, and the central spot is from the central part of the input beam that passes through a 2.5 mm diameter hole in the center of the axicon. (This hole is used in experiments where secondary delayed pulses are injected through the axicon and coupled into the plasma waveguide and optically guided [8,18].) Visually, Bessel beam breakdowns of the clustered gas jet are significantly brighter than similar breakdowns in unclustered jets or in backfill targets.

The time- and space-resolved evolution of the plasma waveguide is measured by a probe pulse directed perpendicularly to the waveguide axis and into a folded wave front interferometer [23] (see Fig 1). The probe was obtained by splitting off a 1 mJ portion of the 100 ps main pulse and directing it to an optical delay line, which provides the time resolution through pump-probe delays of −1 ns through +11 ns. The diameter of the probe beam 1.6 cm, which was big enough to fully contain the plasma channel. After passing through the plasma channel, the probe was directed to a lens pair imaging system with the first lens of focal length f1 placed a distance f1 away from the plasma, the second lens (f2) placed a distance f1+f2 away from the first lens, and the probe image formed a distance f2 beyond the second lens with magnification f2/f1=2. An uncoated BK7 wedge in the probe beam path prior to the image plane was used to produce two angularly separated beams. At the image plane the two beams form complementary interferograms whereby a portion of the beam unperturbed by the plasma overlaps with a portion of the beam passing through the plasma to generate

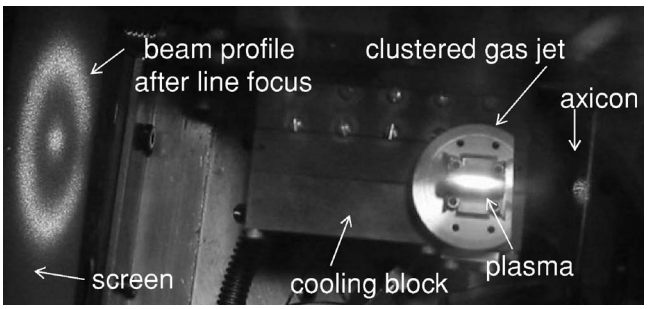

FIG. 4. An image of the Bessel beam-induced breakdown occurring in an elongated argon cluster jet. The ring on the screen at left is the nonlinear fluorescence of the locus of rays from the axicon transmitted through the plasma. The central spot is from the central part of the input beam that passes through a 3 mm diameter central hole in the axicon.

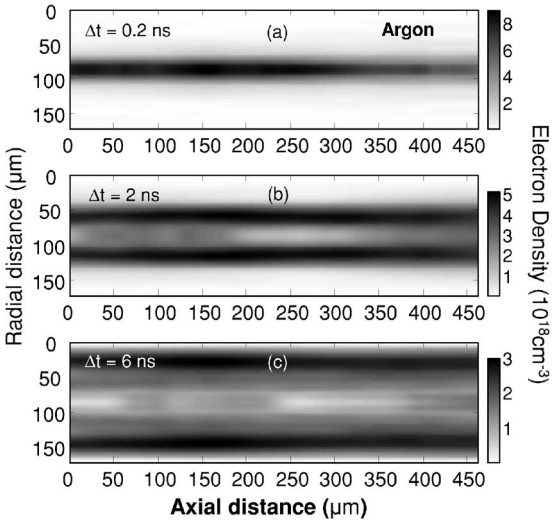

FIG. 5. Gray scale images of the extracted electron density near the center of the waveguide at probe delays (a) 200 ps, (b) 2 ns, and (c) 6 ns for argon at a backing pressure of 800 psi, valve temperature of 173 K, and pump laser energy of 150 mJ.

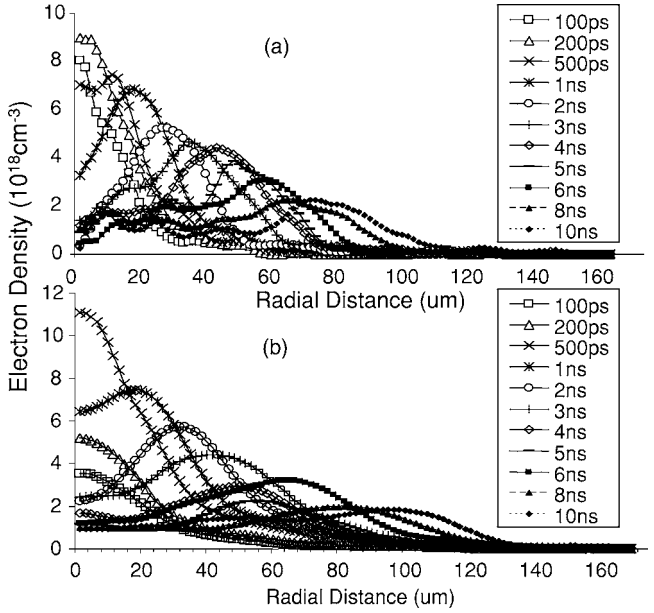

FIG. 6. Extracted electron density versus radius near the central region of the waveguide as a function of probe delay for argon cluster jets with valve temperature 173 K, backing pressure 800 psi, and pump laser energy 150 mJ; (b) valve temperature of 173 K, backing pressure 500 psi, and pump laser energy 230 mJ.

interference fringe shifts due to the plasma refractive index profile. At the image plane a 4× microscope objective coupled to CCD camera was used to capture the interferogram, for an overall system magnification of 8×. The phase information encoded in the interferogram was extracted with a fast Fourier transform technique, and the phase was further processed by Abel inversion, assuming cylindrical symmetry, to recover electron density profiles [23–25]. Insets to Fig. 1 show typical interferograms of the central region of the waveguide and the end.

III. EXPERIMENTAL RESULTS

Figures 5(a)–5(c) show gray scale images of the extracted electron density at three probe delays for the case of argon at valve temperature 173 K, backing pressure of 800 psi, and pump laser energy of 150 mJ. It is notable that for waveguides produced in nonclustered argon, the typical pump energy required was ~500 mJ *and* a seed gas (N_2O at 10%–20% partial pressure) was needed to provide OFI electrons to seed the avalanche breakdown [23]. In the present case, the lower laser energy and lack of a seed gas means a much reduced OFI rate. But the much higher local atomic density in a cluster ensures that, even with the lower yields of first generation OFI electrons, the subsequent collisional breakdown is far more vigourous than in the seeded unclustered gas case. This will be seen in the later simulations.

Figure 6 shows plots of electron density versus radius, as a function of probe delay from the central region of the waveguide, for two settings of the argon cluster jet. In Fig. 6(a), $P_{\text{valve}}=800$ psi, $T_{\text{valve}}=173$ K, and laser energy is 150 mJ. By ~500 ps, a hollow electron density profile develops, and a laser-induced shock wave propagates radially outward. By 2 ns, the on-axis electron density has dropped below $\sim 10^{18}$ cm^{-3}. The electron density falloff at radial distances beyond the shock is more extended than for laser-plasmas generated in unclustered targets, owing to both conduction and radiation precursors [26,27] and a reduced laser intensity threshold for strong ionization of clusters [15]. The latter effect enables subsidiary off-axis radial maxima of the Bessel beam to be effective in plasma generation. In Fig. 6(b), P_{valve} was reduced to 500 psi, also with $T_{\text{valve}}=173$ K. In order to make a stable, continuous channel, it was necessary to increase the pump laser energy to 230 mJ. Under these conditions, it is seen that the peak electron density does not occur until ~500 ps past the pump pulse, and the central electron density dip does not occur until ~1 ns. These results illustrate that cluster target conditions play a significant role in determining the amount of pump energy required for desired waveguide parameters. In this case, increasing the jet backing pressure results in a very large pump energy savings.

We also generated plasma waveguides in a nitrogen cluster jet. Figure 7 shows the evolution of the nitrogen cluster plasma under $P_{\text{valve}}=900$ psi and $T_{\text{valve}}=173$ K with a pump laser energy of 415 mJ. These higher levels of backing pressure and pump energy were required for stable continuous channels. It shows a similar evolution as in the argon cluster plasma, with the density dip appearing at ~500 ps, and the central density dropping to $<10^{18}$ cm^{-3} after ~2 ns. By comparison, in unclustered nitrogen, both from gas jets and in backfill targets, no breakdown occurred for the pure gas using axicons and 100 ps pulses, and only with significant additional partial pressure of N_2O (>20%) was breakdown possible.

The results of this experiment show that clustered gases achieve breakdown to high degrees of ionization much more readily than unclustered gases. One would expect that an absorption measurement should be consistent with this observation. Such a measurement was performed by collecting

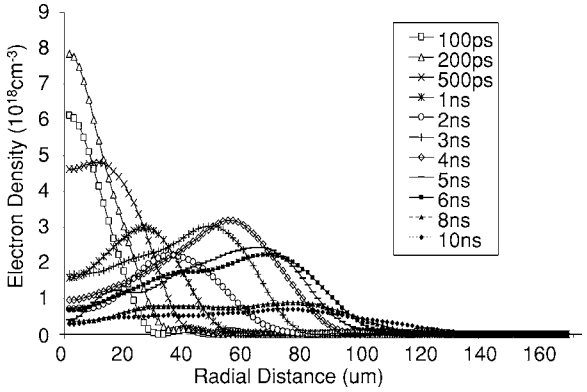

FIG. 7. Electron density versus radius near the central region of the waveguide as a function of probe delay for clustered nitrogen cluster jets with (a) valve temperature 173 K, backing pressure 900 psi, and pump laser energy 415 mJ.

the cone of rays transmitted by the plasma (shown in the schematic of Fig. 1 and shown projected onto the screen in Fig. 4) with a second axicon after the plasma breakdown, and delivering the light to an energy meter. The input beam energy was directed to the axicon by a 90 deg 1064 nm mirror with a central hole of slightly larger diameter than the hole in the axicon. Therefore, for this measurement the central beam spot shown in Fig. 4, which does not participate in plasma generation or heating, was not collected. Figure 8(a) shows absorption versus backing pressure of argon and nitrogen clusters for $T_{\text{valve}}=173$ K and laser energy of 315 mJ and Fig. 8(b) shows absorption as a function of pump energy for argon clusters ($P_{\text{valve}}=800$ psi and $T_{\text{valve}}=173$ K) and for argon gas ($P_{\text{valve}}=800$ psi and $T_{\text{valve}}=298$ K). The level of absorption in unclustered nitrogen jets was below the sensitivity level of the measurement. It is seen that the maximum absorption is approximately 35%. While not at the level of $>80\%$ absorption of femtosecond pulses in clustered gases [13], the absorption of these long 100 ps pulses is much greater than that achievable in unclustered gas jets.

IV. CALCULATIONS OF LONG PULSE BREAKDOWN OF CLUSTER JETS

We now discuss the result that the use of clustered gas significantly enhances pump pulse absorption and waveguide generation, even though the few hundred femtosecond cluster disassembly time is greatly exceeded by our 100 ps pump pulses. Our earlier femtosecond time-resolved measurements showed that heating of few hundred angstrom diameter clusters by 10^{15} W/cm^2, $\lambda=800$ nm, 70 fs pump pulses induces an ultrafast cluster plasma explosion, wherein the peak electron density drops from solid levels of $\sim 10^{23}$ cm^{-3} to subcritical levels below $\sim 2\times 10^{21}$ cm^{-3} within ~ 0.5 ps [15], and the plasmas from nearby cluster explosions merge in $\sim 10-100$ ps, depending on cluster density. The implication of this for the current experiment is that the majority of the 100 ps pulse envelope will encounter low subcritical density, uniform plasma created from expansion and merging of individual cluster explosions that are initiated very early in the pulse. Therefore, an explanation for the surprisingly high absorption efficiency resides in the cluster plasma dynamics in the leading edge of the 100 ps pump pulse.

Figure 9 shows results from our laser cluster hydrodynamic code [28], for a 200 Å argon cluster exposed to a 100 ps, $\lambda=1064$ nm pulse over a range of intensity. The code solves the plasma hydrodynamic equations coupled to the equation $\nabla\cdot(\varepsilon\mathbf{E})=0$ for the electric near-field, where $\varepsilon(\mathbf{r},t)$ is the space- and time-dependent plasma dielectric function and $\mathbf{E}(\mathbf{r},t)$ is the self-consistent electric field from the laser and plasma. The near-field model is well satisfied here for $ka\ll 1$, where k is the laser wave number and a is the cluster radius. The code accounts for OFI and collisional ionization and heating, thermal conduction and uses a time-dependent collisional radiative model for the ionization dynamics. The pulse temporal envelope is taken to be Gaussian. The figure is a semi-log plot of the cluster peak electron density as a function of time for peak pulse intensities in the range $10^{13}-10^{14}$ W/cm^2, corresponding to the range of experimental intensities in the central maximum of the Bessel beam. The pulse starts near $t=-300$ ps at 1.5×10^{-11} of peak intensity (for example, the starting intensity is 1500 W/cm^2 in the case of the peak 10^{14} W/cm^2 pulse), where the initial electron density is taken to be 2 electron/cm^3, effectively zero over the cluster volume. The results are insensitive to this choice of negligible initial electron density. The pulse peaks at $t=0$. It is seen that extremely strong cluster ionization occurs in the far-leading edge of the pulse, saturating to an average degree of ionization $Z_{\text{avg}}\sim 8$ corresponding to the Ne-like Ar^{8+} ion, which is quite stable against further ionization to the next higher stage. The ionization onset time varies

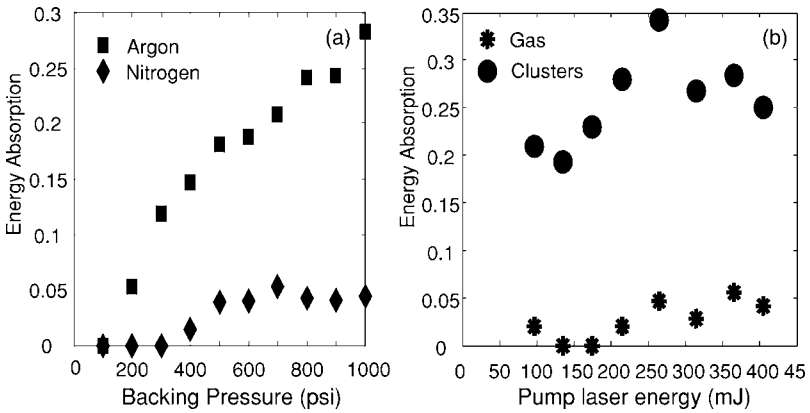

FIG. 8. (a) Absorption efficiency versus backing pressure of clustered argon and nitrogen for temperature 173 K and laser energy 315 mJ; (b) absorption efficiency versus pump laser energy for clustered argon at backing pressure 800 psi and temperature 173 K, and unclustered argon at backing pressure 800 psi and temperature 298 K.

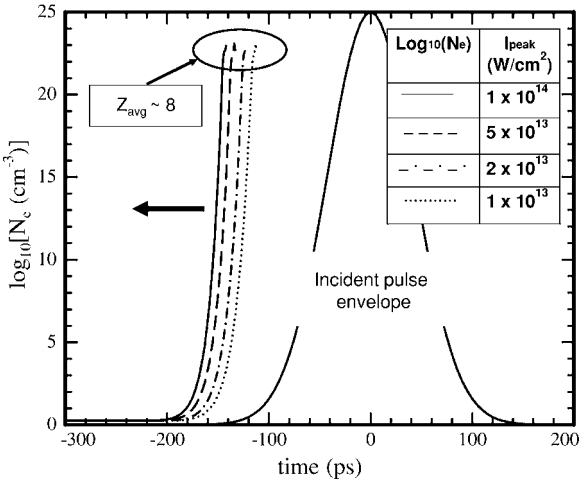

FIG. 9. Calculation using laser-cluster interaction code [28] of the logarithm of electron density versus time for a 200 Å argon cluster under irradiation of 1064 nm, 100 ps pulses of intensity 10^{13}, 2×10^{13}, 5×10^{13}, and 10^{14} W/cm^2. The effective degree of ionization saturates near $Z_{\text{init}}\sim 8$ in the very early leading edge of the pulse.

over a ~40 ps range as the peak intensity varies from 10^{13} to 10^{14} W/cm^2, but the onset always remains in the far-leading edge of the pulse. The exploding cluster plasma, once it has dropped below critical density, can cool by expansion during the leading edge of the long pulse, well before the pulse intensity increases sufficiently to contribute to heating. During this phase, the expanding and merging cluster plasma is also cooled via thermal conduction to the neutrals and weakly preionized gas on the periphery of the main plasma. From single cluster calculations alone [28] (ignoring thermal conduction to the gas jet periphery), expansion cooling can drop the temperature from a peak of a few hundred eV down to a few eV.

The conclusion from these calculations is that essentially the full 100 ps pulse envelope encounters highly ionized, uniform, and relatively cold plasma as its effective initial target. From this perspective, the clustered gas can be viewed as enabling a supercharged preionization scenario. In typical preionization schemes, the initial ionization level per atom is less than unity, $Z_{\text{eff}}\ll 1$ [9,10]. With clusters as the target, one can have $Z_{\text{eff}}\gg 1$, as seen in Fig. 9. The effects of this on the further breakdown and heating of the target can be investigated by utilizing our self-consistent Bessel-beam plasma interaction code [14], which simulates axicon pulse heating of gas-density plasmas. In this calculation, the plasma hydrodynamic equations are solved, coupled to the equation for the z-propagating Bessel beam, $\nabla_\perp{}^2 u+\kappa^2 u=0$, where the electric field is given by $E(\mathbf{r}_\perp,z,\omega)=e^{i\beta z}u(\mathbf{r}_\perp,\omega)$, $\kappa^2(\mathbf{r}_\perp,\omega)=k^2[1+\delta_{plasma}(\mathbf{r}_\perp,\omega)+4\pi\chi(\mathbf{r}_\perp,\omega)]-\beta^2$ is the square of the local transverse wave number, χ is the total atomic and ionic susceptibility, and δ_{plasma} is the plasma contribution to the medium response. In the above equations, $\nabla_\perp{}^2$ is the Laplacian in the transverse coordinate $\mathbf{r}_\perp$, $k=\omega/c$ is the vacuum wave number of the laser, and β is the wave number along the propagation axis z.

For this calculation, we use conditions corresponding to experimental parameters of Fig. 8: axicon ray approach angle $\gamma=15$ deg, $\lambda=1064$ nm, a peak intensity of 2.5×10^{13} W/cm^2, and gas densities $N_n=0.7\times10^{19}$, 1.0×10^{19}, and 1.4×10^{19} cm^{-3}, corresponding to backfill

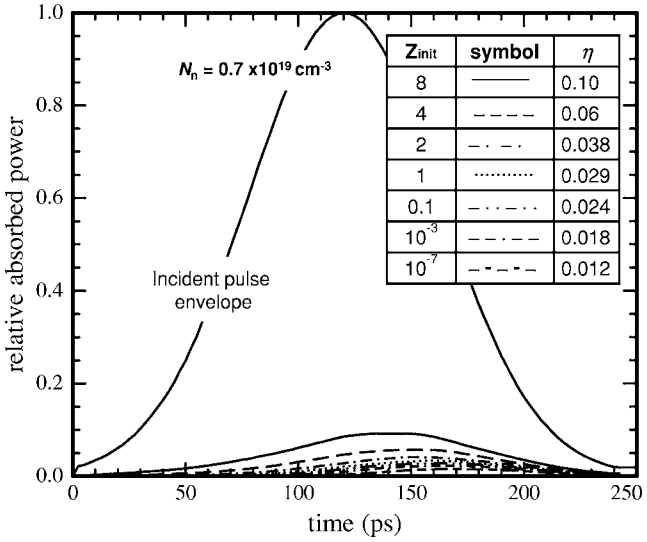

FIG. 10. Calculation using self-consistent Bessel-beam plasma interaction code [14] of time-dependent Bessel beam absorption. The initial ionization state is varied from $Z_{\text{init}}=10^{-7}$ to $Z_{\text{init}}=8$, corresponding to the conditions encountered by a long pulse interacting with a range of targets spanning initially unclustered gas to a gas of large clusters. The initial gas density is 0.7×10^{19} cm^{-3} (200 Torr). Total absorption is given by η. Here, the absorption for $Z_{\text{init}}=8$ ("clustered") is ~10 times greater than for $Z_{\text{init}}\sim10^{-7}$ ("unclustered").

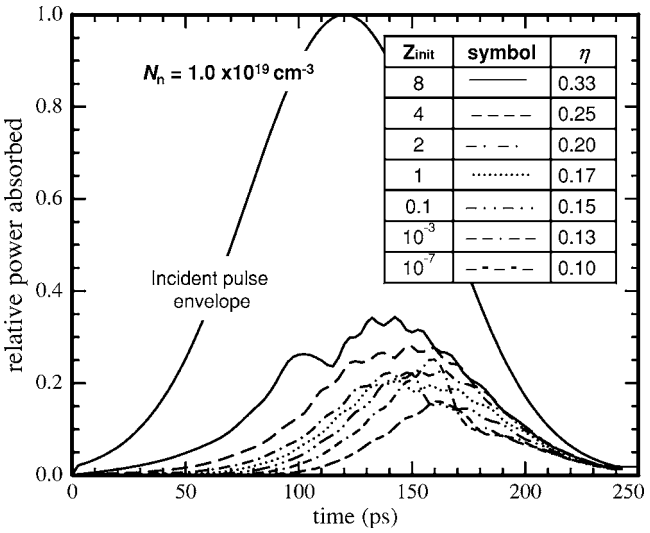

FIG. 11. Calculation using self-consistent Bessel-beam plasma interaction code [14] of time-dependent Bessel beam absorption. The initial ionization state is varied from $Z_{\text{init}}=10^{-7}$ to $Z_{\text{init}}=8$, corresponding to the conditions encountered by a long pulse interacting with a range of targets spanning initially unclustered gas to a gas of large clusters. The initial gas density is 1.0×10^{19} cm^{-3} (300 Torr). Total absorption is given by η. Here, the maximum absorption of ~35% is predicted for the $Z_{\text{init}}=8$ ("clustered") case.

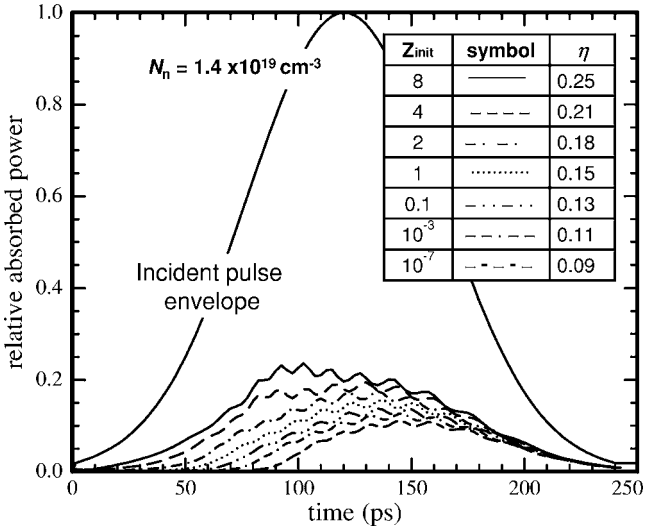

FIG. 12. Calculation using self-consistent Bessel-beam plasma interaction code [14] of time-dependent Bessel beam absorption. The initial ionization state is varied from $Z_{init}=10^{-7}$ to $Z_{init}=8$, corresponding to the conditions encountered by a long pulse interacting with a range of targets spanning initially unclustered gas to a gas of large clusters. The initial gas density is 1.4×10^{19} cm^{-3} (400 Torr). Total absorption is given by η. Here, the absorption drops compared to the 1.0×10^{19} cm^{-3} case (Fig. 11) because the Bessel beam experiences incipient exclusion from the central region of the plasma.

pressures of 200, 300, and 400 Torr, and shown in Figs. 10–12, respectively. The figures show the time-dependent absorption for initial ionization levels in the range $Z_{init}=10^{-7}$ through $Z_{init}=8$. This corresponds to the initial plasma conditions encountered by a long pulse interacting with targets spanning the range of initially unclustered gas to a gas of large clusters. Overlaid on these curves is the incident pulse envelope, normalized to unity. The tables inset in the plots give the curve legend for the various values of Z_{init} and the total absorption fraction, η, which is the integral of each curve. It is seen for 200 Torr (Fig. 10) that absorption for the "clustered" case of $Z_{init}=8$ ($\eta=0.10$) is ten times greater than for the "unclustered" case of $Z_{init}=10^{-7}$ ($\eta=0.012$). For 300 Torr (Fig. 11), the maximum absorption is $\eta=0.33$, while it decreases at 400 Torr (Fig. 12) to $\eta=0.25$. In both the latter cases, a high degree of initial ionization increases the subsequent absorption by approximately a factor of 3 compared to the low initial ionization case. In the higher-density case, the absorption is somewhat less, owing to the incipient exclusion of the axicon field from the plasma caused by the increase in the effective critical density $N_{cr,eff}=N_{cr}\sin^2\gamma$ seen by the Bessel beam [14]. In general, low average density cluster gases show the greatest relative absorption enhancement over their nonclustered counterparts, while the largest absolute absorption takes place at intermediate pressures, before density is large enough to effect Bessel-beam field exclusion. In all cases the absorption in clustered gases, represented by the $Z_{init}\gg1$ cases, is significantly greater than in neutral gases of equivalent average density, where conventional preionization $Z_{init}\ll1$.

V. CONCLUSIONS

We have demonstrated that clustered gases are an excellent medium for use in plasma waveguide generation using long pulse Bessel beams. The resulting waveguides can have both low central density and small diameter, a desirable but hard to achieve combination for hydrodynamic shock waveguides using conventional gases, or for other techniques such as discharge capillaries. A main advantage for which cluster targets are well known, namely extremely efficient absorption of femtosecond laser pulses, is shown to extend to pulses that are significantly longer than the time scale for cluster explosive disassembly. This is due to the fact that a clustered gas is very strongly preionized in the far-leading edge of a long pulse; the subsequent pulse envelope acts to heat a uniform, cool plasma that is already near ionization saturation.

ACKNOWLEDGMENTS

The authors thank Andy York for help with improving the analysis programs, and also thank E. Parra and J. Fan for help with the cluster jet cooling block design. This work is supported by the U.S. Department of Energy and the National Science Foundation.

[1] T. Tajima and J. M. Dawson, Phys. Rev. Lett. **43**, 267 (1979); P. Sprangle, E. Esarey, A. Ting, and G. Joyce, Appl. Phys. Lett. **53**, 2146 (1988).

[2] E. Esarey, P. Sprangle, and A. Ting, IEEE Trans. Plasma Sci. **24**, 252 (1996); C. J. Joshi and P. B. Corkum, Phys. Today **48**, 36 (1995).

[3] H. M. Milchberg, C. G. Durfee III, and T. J. McIlrath, Phys. Rev. Lett. **75**, 2494 (1995); P. L. Shkolnikov, A. E. Kaplan, and A. Lago, J. Opt. Soc. Am. B **13**, 412 (1996).

[4] A. Butler, A. J. Gonsalves, C. M. McKenna, D. J. Spence, S. M. Hooker, S. Sebban, T. Mocek, I. Bettaibi, and B. Cros, Phys. Rev. Lett. **91**, 205001 (2003); H. M. Milchberg, C. G. Durfee III, and J. Lynch, J. Opt. Soc. Am. B **12**, 731 (1995).

[5] A. Butler, D. J. Spence, and S. M. Hooker, Phys. Rev. Lett. **89**, 185003 (2002).

[6] Y. Erlich, C. Cohen, and A. Zigler, Phys. Rev. Lett. **77**, 4186 (1996); D. Kaganovich, D. Kaganovich, A. Ting, C. I. Moore, A. Zigler, H. R. Burns, Y. Ehrlich, R. Hubbard, and P. Sprangle, Phys. Rev. E **59**, R4769 (1999).

[7] B. M. Luther,Y. Wang, M. C. Marconi, J. L. A. Chilla, M. A. Larotonda, and J. J. Rocca, Phys. Rev. Lett. **92**, 235002 (2004).

[8] C. G. Durfee III and H. M. Milchberg, Phys. Rev. Lett. **71**, 2409 (1993); S. P. Nikitin, I. Alexeev, J. Fan, and H. M. Milchberg, Phys. Rev. E **59**, R3839 (1999).

[9] P. Volfbeyn, E. Esarey, and W. P. Leemans, Phys. Plasmas **6**,

2269 (1999).
[10] E. W. Gaul, S. P. LeBlanc, A. R. Lundquist, R. Zgadzaj, H. Langoff, and M. C. Downer, Appl. Phys. Lett. **77**, 4112 (2000).
[11] K. Krushelnick, A. Ting, C. I. Moore, H. R. Burris, E. Esarey, P. Sprangle, and M. Baine, Phys. Rev. Lett. **78**, 4047 (1997); S.-Y. Chen, G. S. Sarkisov, A. Maksimchuk, R. Wagner, and D. Umstadler, *ibid.* **80**, 2610 (1998).
[12] I. Alexeev, T. M. Antonsen, K. Y. Kim, and H. M. Milchberg, Phys. Rev. Lett. **90**, 103402 (2003).
[13] V. Kumarappan, K. Y. Kim, and H. M. Milchberg, Phys. Rev. Lett. **94**, 205004 (2005).
[14] J. Fan, E. Parra, and H. M. Milchberg, Phys. Rev. Lett. **84**, 3085 (2000); J. Fan, E. Parra, K. Y. Kim, I. Alexeev, H. M. Milchberg, J. Cooley, and T. M. Antonsen, Phys. Rev. E **65**, 056408 (2002).
[15] K. Y. Kim, I. Alexeev, E. Parra, and H. M. Milchberg, Phys. Rev. Lett. **90**, 023401 (2003).
[16] M. V. Ammosov, N. B. Delone, and V. P. Krainov, Sov. Phys. JETP **64**, 1191 (1987) [Zh. Eksp. Teor. Fiz. **91**, 2008 (1986)].
[17] K. Y. Kim, I. Alexeev, J. Fan, E. Parra, and H. M. Milchberg, AIP Conf. Proc. **647**, 646 (2002).
[18] C. G. Durfee III, J. Lynch, and H. M. Milchberg, Phys. Rev. E **51**, 2368 (1995).
[19] W. P. Leemans, P. Volfbeyn, K. Z. Guo, S. Chattopadhyay, C. B. Schroeder, B. A. Shadwick, P. B. Lee, J. S. Wurtele, and E. Esarey, Phys. Plasmas **5**, 1615 (1998).
[20] O. F. Hagena and W. Obert, J. Chem. Phys. **56**, 1793 (1972); O. F. Hagena, Z. Phys. D: At., Mol. Clusters **4**, 291 (1987).
[21] E. Parra, S. J. McNaught, and H. M. Milchberg, Rev. Sci. Instrum. **73**, 468 (2002).
[22] K. Y. Kim, V. Kumarappan, and H. M. Milchberg, Appl. Phys. Lett. **83**, 3210 (2003).
[23] T. R. Clark and H. M. Milchberg, Phys. Rev. Lett. **78**, 2373 (1997).
[24] M. Takeda, H. Ina, and S. Kobayashi, J. Opt. Soc. Am. **72**, 156 (1981).
[25] I. H. Hutchinson, *Principles of Plasma Diagnostics* (Cambridge University Press, Cambridge, 1987).
[26] J. Fan, T. R. Clark, and H. M. Milchberg, Appl. Phys. Lett. **73**, 3064 (1998).
[27] T. Ditmire, E. T. Gumbrell, R. A. Smith, A. Djaoui, and M. H. R. Hutchinson, Phys. Rev. Lett. **80**, 720 (1998).
[28] H. M. Milchberg, S. J. McNaught, and E. Parra, Phys. Rev. E **64**, 056402 (2001).